Published by :
http://www.ijert.org

International Journal of Engineering Research & Technology (IJERT)
ISSN: 2278-0181
Vol. 14 Issue 10, October - 2025

Improving Visible Light Driven Photocatalytic Performance of $ZnWO_4/g\text{-}C_3N_4$ Nanocomposites for RhB Dye Degradation

T. Prabhuraj
Advanced Nanomaterials and Energy Research Laboratory,
Department of Energy Science and Technology,
Periyar University, Salem – 636011, Tamil Nadu

A. Gomathi
Department of Physics, School of Maritime Studies,
Vels Institute of Science, Technology and Advanced Studies, Thalambur, Chennai – 600 130, Tamil Nadu,

P. Maadeswaran
Advanced Nanomaterials and Energy Research Laboratory,
Department of Energy Science and Technology, Periyar University, Salem - 636011, Tamil Nadu

***Abstract*—This study attempts to break down Rhodamine dye with $ZnWO_4$@CN nanocomposites for environmental use. The nanocomposites were made using a simple hydrothermal process and examined for optical, structural, and morphological properties. XPS, SEM-EDX, UV-DRS, and PL are examples. RhB dye degradation in water was employed to test photocatalytic activity. The study found that $ZnWO_4$@0.5 % CN has superior photocatalytic performance compared to pure $ZnWO_4$, $ZnWO_4$@0.1% CN, and ZnWO4@1.0 % CN nanocomposites. The synergistic effect results from efficient photoinduced electron-hole pair separation and transfer. As an excellent electron conductor, activated carbon increases charge separation and extends charge carrier life. Photocatalytic experiments indicated $ZnWO_4$@0.5 % CN nanocomposites destroyed 97% RhB dye in 150 minutes. Quenching investigations confirmed that the degradation kinetics followed a pseudo-first-order model, indicating that reactive oxygen species (ROS) formed efficiently and abundantly caused dye degradation.**

***Keywords*—Reactive oxygen species, Kinetics, Charge separation, Synergistic effect, Rhodamine dye**

I. INTRODUCTION

Industrialization and population growth have contributed to environmental pollution and energy shortages caused by organic pollutants, which have become major barriers to economic and social progress [1, 2]. The adoption of pollution-free technologies and the identification of clean energy sources are crucial for achieving sustainable development [3, 4]. In contrast, organic dyes used widely in sectors like food, cosmetics, and paint industries are thought of as a significant source of water pollution [5]. Rhodamine B (RhB) is a yellow anthracene dye that is very soluble, has excellent brightness, and finds widespread use in biological applications and industrial production processes [6, 7]. Several health problems, including nausea, skin irritation, and vomiting, can be caused by exposure to high concentrations of RhB [8, 9]. Chemically durable, hardly biodegradable, and extremely toxic even at low concentrations—RhB is a synthetic organic dye. They are extremely dangerous for people and the environment [10]. So, to degrade organic contaminants, we need an effective, inexpensive method. Due to its capacity to fully mineralize the organic contaminants, semiconductor photocatalyst have garnered tremendous interest among researchers [11]. A wide band gap and a fast electron-hole (e-h) pair recombination rate are two limitations of the widely used semiconductor photocatalyst that contribute to its poor efficiency in converting light into energy [12]. Developing photo catalytical technology currently hinges on perfecting the synthesis of photocatalysts, which must possess attributes including low production costs, wide light absorption ranges, high cycle stability, and outstanding catalytic activity [13]. Consequently, it is of the utmost importance to develop an environmentally friendly and exceptionally effective photocatalyst through the use of standard techniques such as elemental doping, morphological control, and the creation of an appropriate heterojunction structure. A number of parameters determine how well they work, including dimensions, surface charge, shape, thermal characteristics, and optical characteristics [14]. Since narrow band gap oxides absorb a greater amount of visible light and are thought to be better photocatalysts owing to their wide solar light area, researchers are concentrating on employing these materials for photocatalysis [15]. Zinc tungstate ($ZnWO_4$) stands out among narrow band gap semiconductors due to its exceptional optical, electrical, structural, and physiochemical characteristics; these qualities make it a great candidate for use in composites and open up new avenues for environmental applications [16].Research on $ZnWO_4$, a wolframite tungstate metal oxide with a d10s2-d10 electronic configuration, has been conducted because of its potential uses in water splitting and the breakdown of organic pollutants in water when exposed to UV light [17, 18]. The photocatalytic activity of $ZnWO_4$ is inefficient because it does not absorb visible light [19]. There have been numerous

attempts to increase $ZnWO_4$s photocatalytic activity by harvesting visible light [20, 21].
Under visible light irradiation, g-C_3N_4 may efficiently catalyze photochemical processes because to its low bandgap of about 2.8 eV [22, 23]. Attaching Co nanoclusters to g-C_3N_4 allowed Shang et al. to investigate their potential for CO2 reduction with great success [24, 25]. By adding nitrogen vacancies to g-C3N4, Dong et al. were able to attain high activity in photocatalytic nitrogen fixation [26]. The issue that single-component $ZnWO_4$ can only use ultraviolet energy is solved when g-C_3N_4 and $ZnWO_4$ are combined because the light absorption range of $ZnWO_4$ is broadened. And since their energy band structures are so similar, g-C_3N_4 is an excellent material for creating heterojunctions with $ZnWO_4$ [27]. The photogenerated carriers will be efficiently segregated and transported under the action of an internal electric field that forms at the composite interface after the composition of g-C_3N_4 and $ZnWO_4$ [28]. Furthermore, a great deal of reducing gases, including NH_3, are produced during the annealing process in a controlled atmosphere when g-C_3N_4 is synthesized using melamine as the precursor. There are a lot of oxygen vacancies in this atmosphere because the oxidation status of W atoms fluctuates [29]. These vacancies can protonate water molecules. Consequently, the combination of g-C_3N_4 and $ZnWO_4$ is able to facilitate effective deprotonation of water molecules, increase the separation of photogenerated carriers, and prolong the light absorption of single-component $ZnWO_4$ [30].
At this time Zinc oxide/graphene oxide heterojunction nanofibers for highly effective photocatalytic nitrogen fixation: Deprotonation of water molecules and photogenerated electrons work in tandem to produce a synergistic impact.
Our goal is to create a composite material by combining $ZnWO_4$ with two-dimensional graphitic carbon nitrate using a hydrothermal process. This approach is heavily influenced by the literature stated earlier. Various analytical techniques were used to thoroughly investigate the proposed catalyst $ZnWO_4$@0.5%CN. Under visible light irradiation, our catalyst $ZnWO_4$/ g-C_3N_4 continuously degraded 97% RhB dye in 150 minutes. The purpose of the scavenger trapping study was to determine whether reactive species were involved in the degradation of the dye. The $ZnWO_4$/ g-C_3N_4 photocatalyst is highly effective in degrading RhB dye in water samples, thanks to its high catalytic efficiency.

II. XRD ANALSYSIS

The 2theta range of 5◦ to 80◦ was used to record the XRD profiles of the nanocomposites in figure 1. These profiles include $ZnWO_4$, g-C_3N_4, $ZnWO_4$@0.1%CN, $ZnWO_4$@0.5%CN, and $ZnWO_4$ @1.0%CN. On planes (100) and (002), respectively, the two diffraction patterns of graphitic carbon nitrate are located at 13◦ and 27.7◦. The JCPDS (03-0401) was entirely in agreement with it [13]. One phase of monoclinic wolframite from the JCPDS (15-0774) has the sharp diffraction peaks of $ZnWO_4$ [23]. The diffraction pattern of the nanocomposite made of $ZnWO_4$ at different mass ratios (0.10% CN, 0.5% CN, and 1.0% CN) shows peaks for $ZnWO_4$, whereas the planes (100), (002), that belong to graphitic carbon nitrate, are absent. We validate the g-C_3N_4 interacts with composite material production in subsequent characterizations.

The broadening of the diffraction peaks, caused by loading activated carbon with $ZnWO_4$ at concentrations of 0.1%, 0.5%, and 1%, reveals the interaction of graphitic carbon nitrate with $ZnWO_4$. The two phases and high crystallinity of $ZnWO_4$@CN nanocomposites were shown by the conspicuous and well-reflected images. Additionally, the absence of any other peaks that are not shown serves as confirmation of the processed materials' purity.

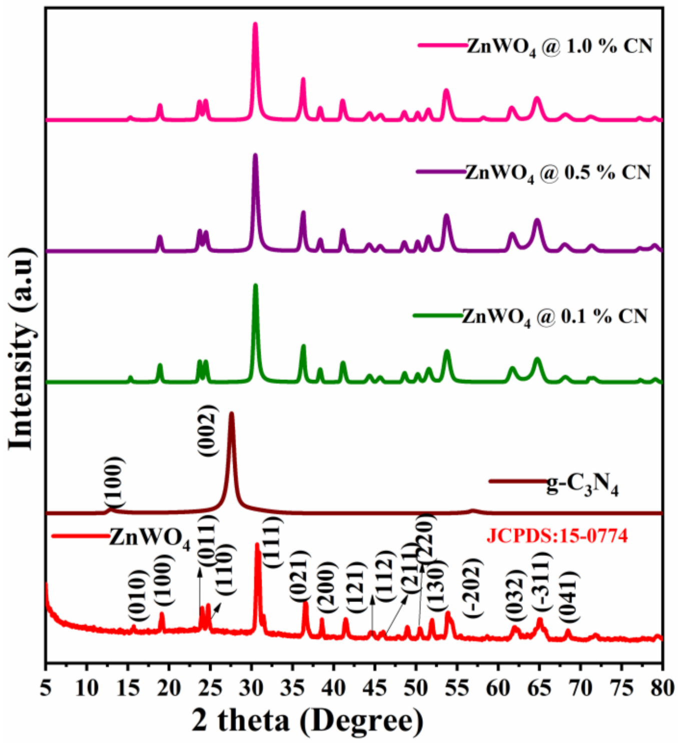

Figure 1. XRD diffraction pattern of $ZnWO_4$, g-C3N4, $ZnWO_4$@0.1%CN, $ZnWO_4$@0.5% CN, $ZnWO_4$@1.0% CN nanocomposite

III. XPS ANALSYSIS

The elemental composition and surface chemical bonding of the as-prepared $ZnWO_4$ @ 1.0% AC crystalline material were shown by the XPS spectra. The survey spectra of the $ZnWO_4$@1.0% CN nanocomposite are shown in Figure 2(a), which validates the presence of carbon, oxygen, zinc, and tungstate. The Zn 2p deconvoluted spectra are shown in
Figure 2(b). Zn 2p3/2 and Zn 2p3/2 belong to the XPS peaks at 1044.5 eV and 1021.5 eV, respectively, according to references [31]. The two main peaks observed in the O1s XPS spectrum at 531.4 eV and 530.4 eV, respectively, are hydroxyl groups, Zn-O-C links between graphitic carbon nitrogen surfaces and $ZnWO_4$, and metal-oxygen-metal bonds, as shown in Figure 2(c) [32]. The high-resolution XPS doublet peaks, which are assigned to W(VI) in WO and can be seen in Figure 3(d) at around 37.1 eV for W 4f 5/2 and 35.2 eV for W 4f 7/2, are presented. At the binding energies of 398.2eV, 399.4 eV, and 400.5 eV, the trinity peaks of N1s are situated [33]. The sp2 hybridized aromatic nitrogen atom bound into carbon (C=N-C) and characterized as Pyrrolilic -N is represented by the first peak. When the tertiary carbon atom forms a bond with the nitrogen atom, as shown by the second peak, the bond is N-

(C)3 [34]. In Figure 3(e), the N-H groups in the graphitic carbon nitrate are shown by the third peak. 70 and 71Two prominent XPS peaks, C=O and C-C, having binding energies of 286.5 eV and 284.6 eV, respectively, make up a C1s spectra shown in Figure 3(f) [35]. In addition, our XPS study verifies that the produced $ZnWO_4$@1.0% CN nanocomposite interacts with graphitic carbon nitrogen surfaces.

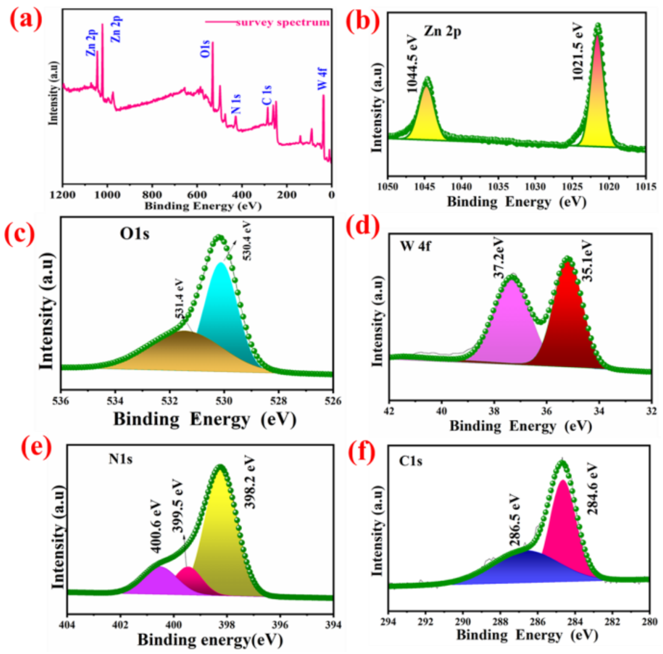

Figure 2. (a) Survey spectra (b-e) Deconvoluted spectra of Zn 2p, O1s, W 4f, N1s, C1s of $ZnWO_4$@0.5%CN nanocomposite.

IV. UV-DRS

The optical features of the $ZnWO_4$, $ZnWO_4$@0.1%CN, $ZnWO_4$@0.5%CN, and $ZnWO_4$@1.0%CN nanocomposites were analyzed using UV-visible absorption spectroscopy. The absorption edge of $ZnWO_4$, $ZnWO_4$@0.1%CN, $ZnWO_4$@0.5%CN, and $ZnWO_4$@1.0%CN nanocomposites is observed at 355 nm, 400 nm, 483 nm, 417 nm respectively. Figure 3(a, c, e, g) shows the absorption spectra of the photocatalyst. Furthermore, the band-gap values were determined utilizing Tauc's plot. The band-gap value for $ZnWO_4$ is 3.5 eV, while the values for $ZnWO_4$@0.1%CN, $ZnWO_4$@0.5%CN, and $ZnWO_4$@1.0%CN nanocomposites are 3.7 eV, 2.72 eV, 2.6 eV, 2.82 eV correspondingly [43,44]. The coupling of $g\text{-}C_3N_4$ diminishes the band gap of $ZnWO_4$ yet enhances the visible light absorption of the $ZnWO_4$@0.5%CN nanocomposite which is shown in figure 3(b, d, f, h). The interaction contact between $g\text{-}C_3N_4$ and $ZnWO_4$ facilitated the frequent and efficient separation of electrons and holes, attributed to the pronounced optical absorption of the $ZnWO_4$@0.5%CN nanocomposite. This leads to enhanced photocatalytic activity and more effective use of the solar spectrum's increased visible light absorption [35].

V. SURFACE AREA ANALYSIS

N_2 adsorption-desorption experiments facilitated the analysis of the pore structure and specific surface area of the $ZnWO_4$@0.5%CN nanocomposites. Figure 4(a-b) illustrates the pore size distributions and N_2 adsorption-desorption isotherms of the synthesized photocatalysts. Figure 5a indicates that the samples exhibit $ZnWO_4$@0.5%CN nanocomposites characteristics of a typical type-IV isotherm. Simultaneously, under IUPAC classifications, the materials exhibit mesoporous structures, evidenced by the isotherm displaying an H3-type hysteresis loop [36]. Moreover, multi-layer adsorption may transpire with increased pressure, while single-molecule

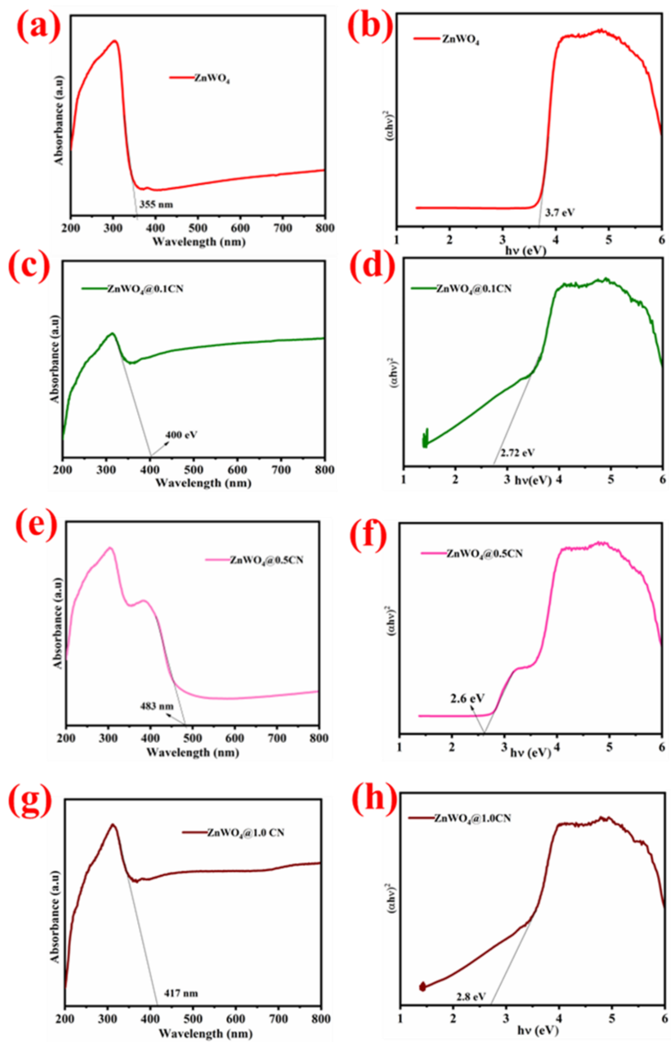

Figure 3. (a-h) UV-DRS and Tauc plot of $ZnWO_4$, $ZnWO_4$@0.1%CN, $ZnWO_4$@0.5%CN, $ZnWO_4$@ 1.0%CN nanocomposite

adsorption occurs at lower relative pressures. Additionally, the isotherm-derived pore diameter, pore volume, and specific surface area are included. Research indicates that the $ZnWO_4$@ 0.5%CN nanocomposite possesses a specific surface area of 94.956 m²/g, with pore diameters and volumes measuring 3.368 nm and 0.079 cc/g, respectively. The mesoporous structure of $ZnWO_4$ @ 0.5%CN nanocomposites enhances the adsorption capacity for organic pollutants in wastewater, accomplished by uniformly distributing $ZnWO_4$ over g-C_3N_4 sheets [37].

Using scanning electron microscopy (SEM), the surface morphology of the synthetic samples was analyzed, as illustrated in Figure 5 (a-i). In the pure $ZnWO_4$ nanoparticles shown in figure 5 (a-d), the surface morphology is rough and porous, and the grains are agglomerated in an uneven shape. Due to the high surface energy of $ZnWO_4$, the particles show non-uniform distribution, suggesting random development and partial aggregation. On the other hand, the $ZnWO_4$/g-C3N4 composite is displayed in the figures 5(e-i), where $ZnWO_4$ nanoparticles are interconnected with sheet-like g-C_3N_4 structures. With these thin stacked sheets present, the surface

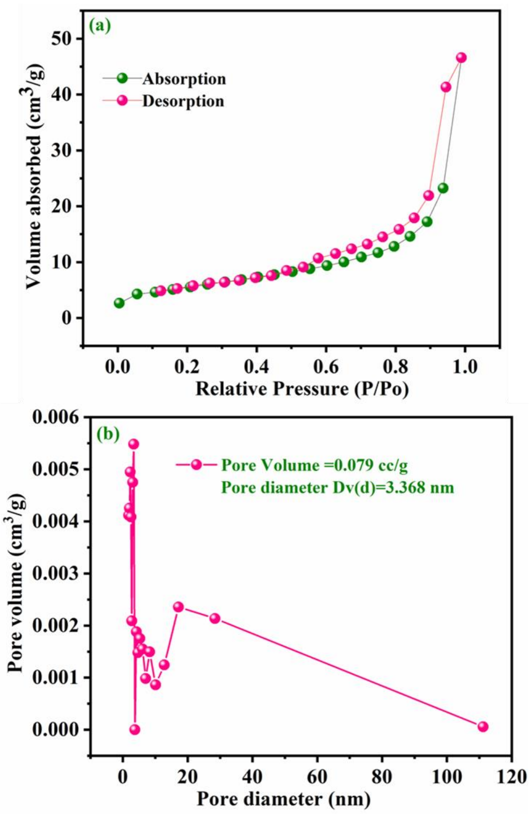

Figure 4. (a, b) Surface area and pore size distribution of $ZnWO_4$@0.5%CN nanocomposites

contact area is increased and the $ZnWO_4$ particles are distributed evenly over the g-C_3N_4. The successful integration of $ZnWO_4$ and g-C_3N_4 into a heterostructure is confirmed by the morphological alteration. The goal of designing this structure is to enhance photocatalytic activity and make charge separation more efficient.

VI. PHOTOCATALYTIC APPLICATIONS

Using Rhodamine B dye molecules as a model pollutant, the photocatalytic degradation efficacy was investigated under visible light. The photodegradation of RhB by various photocatalysts under visible light irradiation from 0 to 150 minutes is illustrated in Figure 6(a-d). Before light irradiation, the dye solution and catalyst combination were placed in darkness for 30 minutes to achieve adsorption-desorption equilibrium. The photocatalysts, whether they were pure $ZnWO_4$ exhibited very little photocatalytic activity during 150 minutes of exposure to visible light. At 150 minutes of irradiation, however, the $ZnWO_4$@0.5%CN photocatalyst demonstrated remarkable degradation efficiency. Based on these results, it seems that the heterojunction of $ZnWO_4$ and g-C3N4 speeds up the breakdown of RhB. Figure 6(a-d) shows the photodegradation rate of RhB for $ZnWO_4$, g-C_3N_4, $ZnWO_4$@0.1%CN, $ZnWO_4$@0.5%CN, and $ZnWO_4$@1.0%CN nanocomposites after 150 minutes of light irradiation; Figure 7 (a-b) shows the corresponding rate constant for the same nanocomposites under visible light illumination and figure 6(a-d) shows the photodegradation rate for $ZnWO_4$, g-C_3N_4, $ZnWO_4$@0.1%CN, $ZnWO_4$@0.5%CN, and $ZnWO_4$@1.0%CN nanocomposites.

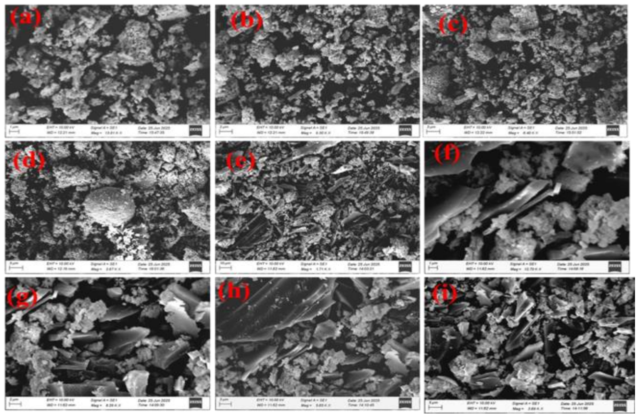

Figure 5. SEM images for (a-d) $ZnWO_4$, (e-i) $ZnWO_4$@0.5% CN nanocomposites

After fitting the degradation data using a pseudo first order kinetic model, the following formula might be used to compute the degradation rates of the different photocatalysts: For every given value of C_0/C, the rate constant kt + x = -ln (C_0/C). A first-order kinetic model is shown in Figure 7b, which depicts the photocatalytic degradation of RhB, after which the relationship between irradiation time (t) and ln (C_0/C) is determined. The kinetic parameter of the $ZnWO_4$@0.5%CN nanocomposites was determined to be 0.0123 min-1 comparison to pure $ZnWO_4$ (0.0059 min-1), $ZnWO_4$@0.1%CN (0.0121 min-1) and $ZnWO_4$@1.0%CN (0.0112min-1), the $ZnWO_4$@0.5%CN nanocomposites exhibited the highest photocatalytic activity (Figure7b).

International Journal of Engineering Research & Technology (IJERT)
ISSN: 2278-0181
Vol. 14 Issue 10, October - 2025

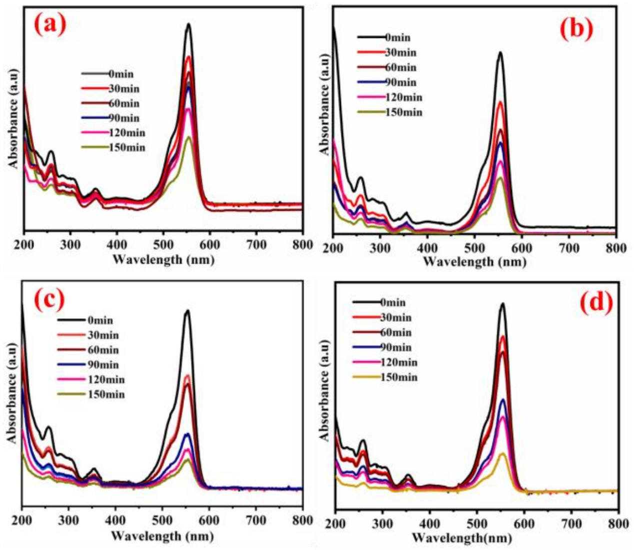

Figure 6. Photocatalytic performance of (a) $ZnWO_4$ (b) $ZnWO_4$ @ 0.1 %CN (c) $ZnWO_4$ @0.5%CN (d) $ZnWO_4$@1.0%CN nanocomposite

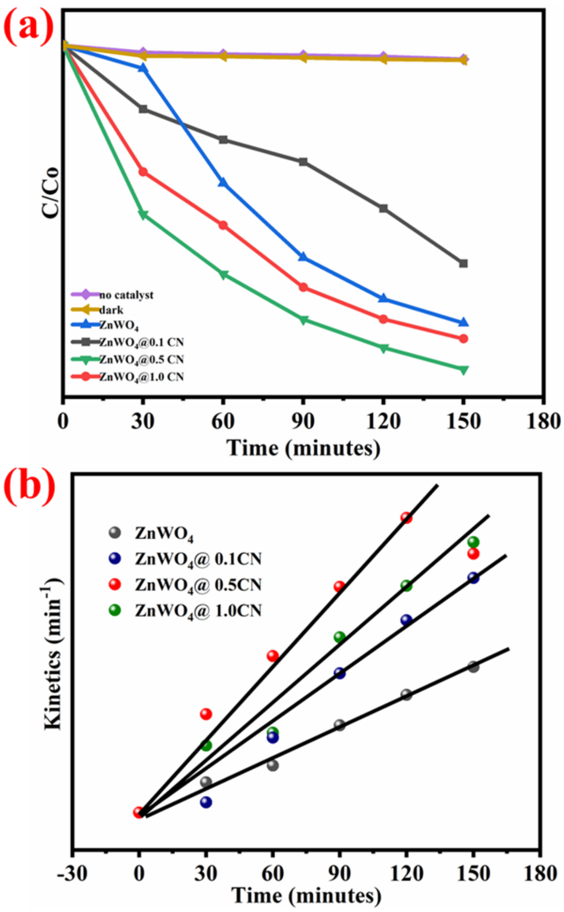

Figure 7. (a) C/Co plot for degradation (b) Kinetics rate constant of $ZnWO_4$@0.5% CN nanocomposites

VII. DURABILITY TEST

For real-world applications, the materials' durability in their prepared state was crucial. Gathering, washing, and drying the material followed the deterioration process. For the following five cycles, the material was exposed to visible light. Also displayed in figure 8 shows the deprivation efficacy, which was determined for the first through fifth cycles in the following order: 97%, 96.8%, 95.4%, 94.8%, and 94.2%. Regarding degrading efficiency, there is a notable disparity. The stability and reusability experiments showed promising results for the $ZnWO_4$@1.0% AC nanocomposite, which might be used for energy recovery and wastewater treatment for environmental remediation [38].

VIII. SCAVENGER TEST

The impact of radical trapping agents on the photodegradation of RhB dyes is examined, as depicted in figure 9. The existence of scavengers in the RhB dye solution signifies the participation of reactive species, implying a progressive decline in degradation efficiency. The use of EDTA significantly diminished the removal effectiveness of the combined dyes from 97% to 26.4% for RhB. The photodegradation of RhB dye, with the inclusion of IPA, BQ and $AgNO_3$, has diminished the degradation efficiency to 39.4% ,74.1% and 80.2%, and respectively. The findings indicate that h^+ significantly contributed to the degradation of

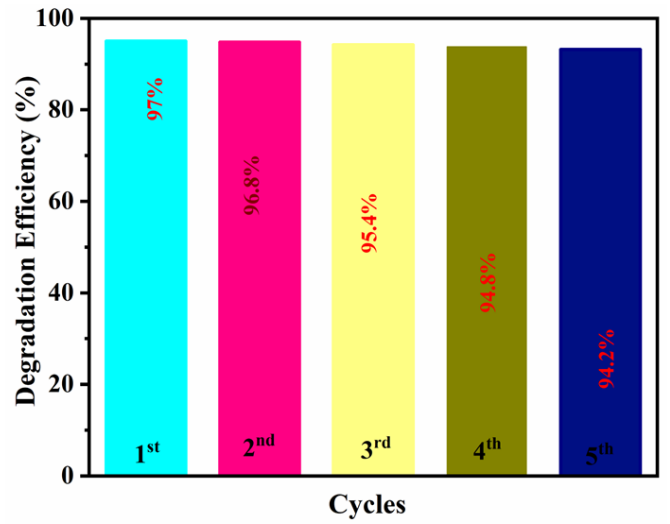

Figure 8. Durability test for $ZnWO_4$@0.5%CN nanocomposites

RhB dye solution. The contribution of active species to the removal of mixed dyes by the $ZnWO_4$/ g-C_3N_4 photocatalyst is ranked as follows: $h^+ > \bullet OH > \bullet O_2 >$ e- [39].

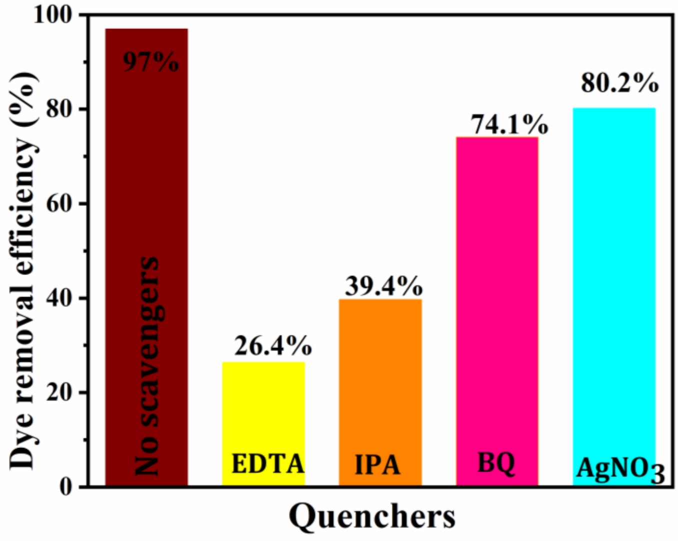

Figure 9. Scavenger test for $ZnWO_4$@0.5%CN nanocomposites

IX. STABILITY ANALYSIS

The stability of the materials was assessed by examining the elemental composition and distinctive peaks of both fresh and used $ZnWO_4$@0.5%CN before to and following the photocatalytic reaction. Figure 10 demonstrates that the distinctive peak remains mostly unaltered following cycling, indicating the stability of the material's structure and the absence of major modification [40].

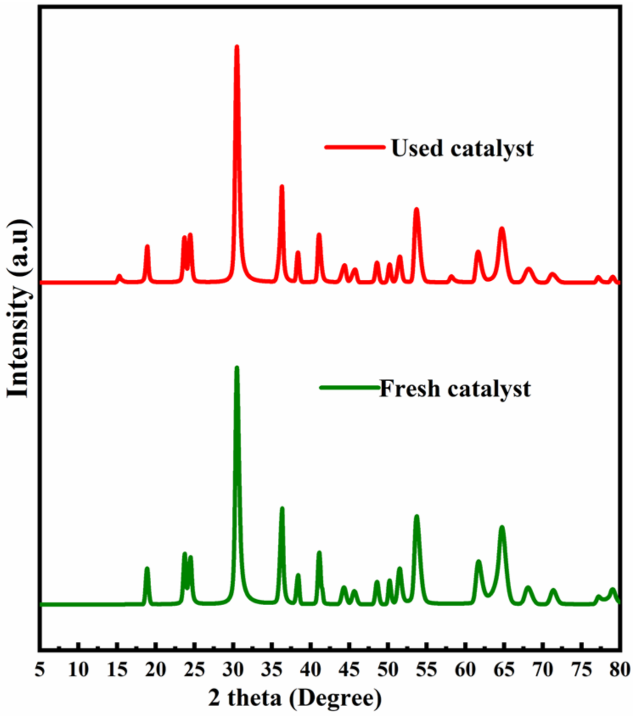

Figure 10. Structural stability test for $ZnWO_4$@0.5% CN nanocomposites

X. CONCLUSION

Photocatalytic materials including $ZnWO_4$ and $ZnWO_4/g\text{-}C_3N_4$ are synthesized in this study with composite ratios of 0.1%, 0.5%, and 1%. Compared to the pure $ZnWO_4$ phase, the g-C_3N_4 loaded composite material has a lower prohibited bandwidth and greater visible light absorption and utilization. When using a photocatalyst to break down RhB dye, $ZnWO_4$@0.5%CN shows the highest catalytic activity. The consumption of the catalyst causes a modest decline in the catalytic effect after five cycles, demonstrating high stability. All of the active groups contribute to the degradation of pollutants, as $\cdot O_2$-, $\cdot$OH, h^+, and e^- are the primary active species in the catalytic process. To sum up, our as-prepared $ZnWO_4$@0.5%CN nanocomposite is environmentally friendly, contains suitable catalytic sites, is easily recyclable, and exhibits remarkable stability. This opens up a new avenue for practical research into the production of visible-light active materials and their potential use in antimicrobial and environmental remediation applications.

REFERENCES

[1] Parasuraman B, Shanmugam P, Barveen NR, et al (2025) Advanced engineering of smart nanomaterials: ZnWO4/CoWO4/g-C3N4 heterojunction photocatalysts for environmental and biomedical application. J Alloys Compd 1010:178200. https://doi.org/10.1016/j.jallcom.2024.178200
[2] Shetty SS, D D, S H, et al (2023) Environmental pollutants and their effects on human health. Heliyon 9:e19496. https://doi.org/10.1016/j.heliyon.2023.e19496
[3] Zhang C, Khorshidi H, Najafi E, Ghasemi M (2023) Fresh, mechanical and microstructural properties of alkali-activated composites incorporating nanomaterials: A comprehensive review. J Clean Prod 384:135390. https://doi.org/10.1016/j.jclepro.2022.135390
[4] Kumar R, Raizada P, Verma N, et al (2021) Recent advances on water disinfection using bismuth based modified photocatalysts: Strategies and challenges. J Clean Prod 297:126617. https://doi.org/10.1016/j.jclepro.2021.126617
[5] Kumar M, Singh NK, Kumar RS, Singh R (2024) Production of Green Hydrogen through Photocatalysis. pp 1–24
[6] Fan Y, He C, Li Y (2022) Iron oxide clusters on g-C3N4 promote the electron–hole separation in photo-Fenton reaction for efficient degradation of wastewater. Chemical Papers 76:7553–7563. https://doi.org/10.1007/s11696-022-02419-2
[7] Barveen NR, Parasuraman B, Wang P-Y, et al (2024) Facile construction of ZnWO4/g-C3N4 heterojunction for the improved photocatalytic degradation of MB, RhB and mixed dyes. Surfaces and Interfaces 53:105039. https://doi.org/10.1016/j.surfin.2024.105039
[8] Ghorui UK, Mondal P, Satra J, et al (2022) In situ metallic copper incorporation into novel g-C3N4/ZnWO4 nanocomposite semiconductor for efficient thin film solar cell application. Mater Sci Semicond Process 143:106559. https://doi.org/10.1016/j.mssp.2022.106559
[9] Sun L, Zhao X, Jia C-J, et al (2012) Enhanced visible-light photocatalytic activity of g-C3N4–ZnWO4 by fabricating a heterojunction: investigation based on experimental and theoretical studies. J Mater Chem 22:23428. https://doi.org/10.1039/c2jm34965e
[10] Wang X, Lin S, Cui N, et al (2024) Synthesis of ZnWO4/NiWO4 photocatalysts and their application in tetracycline hydrochloride degradation and antibacterial activities. J Taiwan Inst Chem Eng 157:105408. https://doi.org/10.1016/j.jtice.2024.105408
[11] Mohamed MM, Khairy M, Eid S (2018) Polyethylene glycol assisted one-pot hydrothermal synthesis of NiWO4/WO3 heterojunction for direct Methanol fuel cells. Electrochim Acta 263:286–298. https://doi.org/10.1016/j.electacta.2018.01.063
[12] Huang G, Zhang C, Zhu Y (2007) ZnWO4 photocatalyst with high activity for degradation of organic contaminants. J Alloys Compd 432:269–276. https://doi.org/10.1016/j.jallcom.2006.05.109
[13] Li Y, Wang J (2024) 2D/2D Z -scheme $WO_3/g\text{-}C_3N_4$ heterojunctions for photocatalytic organic pollutant degradation and nitrogen fixation. Mater Adv 5:749–761. https://doi.org/10.1039/D3MA00915G
[14] Zhu X, Wang L, Feng C, et al (2024) Z-scheme CoWO4/g-C3N4 heterojunction for enhanced ultraviolet-light-driven photocatalytic activity towards the degradation of tetracycline. Journal of Materials Science: Materials in Electronics 35:2036. https://doi.org/10.1007/s10854-024-13809-5

[15] Wu Y, Zhou S, He T, et al (2019) Photocatalytic activities of ZnWO4 and Bi@ZnWO4 nanorods. Appl Surf Sci 484:409–413. https://doi.org/10.1016/j.apsusc.2019.04.116
[16] Li Y, Zhou F, Zhu Z, Wu F (2019) Inactivating marine microorganisms for photoelectrocatalysis by ZnWO4 electrode obtained by surfactant-assisted synthesis. Appl Surf Sci 467–468:819–824. https://doi.org/10.1016/j.apsusc.2018.10.186
[17] Pan Y-M, Zhang W, Hu Z-F, et al (2019) Synthesis of Ti4+-doped ZnWO4 phosphors for enhancing photocatalytic activity. J Lumin 206:267–272. https://doi.org/10.1016/j.jlumin.2018.10.054
[18] Li M, Zhu Q, Li J-G, Kim B-N (2020) Elongation of ZnWO4 nanocrystals for enhanced photocatalysis and the effects of Ag decoration. Appl Surf Sci 515:146011. https://doi.org/10.1016/j.apsusc.2020.146011
[19] Abubakar HL, Tijani JO, Abdulkareem SA, et al (2022) A review on the applications of zinc tungstate (ZnWO4) photocatalyst for wastewater treatment. Heliyon 8:e09964. https://doi.org/10.1016/j.heliyon.2022.e09964
[20] Wu Y, Tie J, Chen C, et al (2019) Synthesis of LAS/ZnO/ZnWO4 3D rod-like heterojunctions with efficient photocatalytic performance: Synergistic effects of highly active site exposure and low carrier recombination. Ceram Int 45:13656–13663. https://doi.org/10.1016/j.ceramint.2019.04.027
[21] Neto NFA, Nunes TBO, Li M, et al (2020) Influence of microwave-assisted hydrothermal treatment time on the crystallinity, morphology and optical properties of ZnWO4 nanoparticles: Photocatalytic activity. Ceram Int 46:1766–1774. https://doi.org/10.1016/j.ceramint.2019.09.151
[22] Huang Y, Gao Y, Zhang Q, et al (2016) Hierarchical porous ZnWO4 microspheres synthesized by ultrasonic spray pyrolysis: Characterization, mechanistic and photocatalytic NO removal studies. Appl Catal A Gen 515:170–178. https://doi.org/10.1016/j.apcata.2016.02.007
[23] Dai M, He Z, Zhang P, et al (2022) ZnWO4-ZnIn2S4 S-scheme heterojunction for enhanced photocatalytic H2 evolution. J Mater Sci Technol 122:231–242. https://doi.org/10.1016/j.jmst.2022.02.014
[24] Zhuang H, Xu W, Lin L, et al (2019) Construction of one dimensional ZnWO4@SnWO4 core-shell heterostructure for boosted photocatalytic performance. J Mater Sci Technol 35:2312–2318. https://doi.org/10.1016/j.jmst.2019.05.036
[25] Yuan K, Cao Q, Li X, et al (2017) Synthesis of WO3@ZnWO4@ZnO-ZnO hierarchical nanocactus arrays for efficient photoelectrochemical water splitting. Nano Energy 41:543–551. https://doi.org/10.1016/j.nanoen.2017.09.053
[26] Dutta DP, Raval P (2018) Effect of transition metal ion (Cr 3+ , Mn 2+ and Cu 2+) doping on the photocatalytic properties of ZnWO 4 nanoparticles. J Photochem Photobiol A Chem 357:193–200. https://doi.org/10.1016/j.jphotochem.2018.02.026
[27] Dutta DP, Ramakrishnan M, Roy M, Kumar A (2017) Effect of transition metal doping on the photocatalytic properties of FeVO4 nanoparticles. J Photochem Photobiol A Chem 335:102–111. https://doi.org/10.1016/j.jphotochem.2016.11.022
[28] Wei L, Zhang H, Cao J (2019) Electrospinning of Ag/ZnWO4/WO3 composite nanofibers with high visible light photocatalytic activity. Mater Lett 236:171–174. https://doi.org/10.1016/j.matlet.2018.10.088
[29] Ma D, Yang L, Sheng Z, Chen Y (2021) Photocatalytic degradation mechanism of benzene over ZnWO4: Revealing the synergistic effects of Na-doping and oxygen vacancies. Chemical Engineering Journal 405:126538. https://doi.org/10.1016/j.cej.2020.126538
[30] Wang X, Yu S, Li Z-H, et al (2021) Fabrication Z-scheme heterojunction of Ag2O/ZnWO4 with enhanced sonocatalytic performances for meloxicam decomposition: Increasing adsorption and generation of reactive species. Chemical Engineering Journal 405:126922. https://doi.org/10.1016/j.cej.2020.126922
[31] Selvamani M, Alsulmi A, Sundaramoorthy A, et al (2023) Synthesis of ZnWO4 nanorods: the photocatalytic effects on RhB dye degradation upon irradiation with sunlight light. Journal of Materials Science: Materials in Electronics 34:2094. https://doi.org/10.1007/s10854-023-11513-4
[32] Kumar P, Verma S, Korošin NČ, et al (2022) Increasing the photocatalytic efficiency of ZnWO4 by synthesizing a Bi2WO6/ZnWO4 composite photocatalyst. Catal Today 397–399:278–285. https://doi.org/10.1016/j.cattod.2021.09.012
[33] Paul DR, Gautam S, Panchal P, et al (2020) ZnO-Modified g-C_3N_4: A Potential Photocatalyst for Environmental Application. ACS Omega 5:3828–3838. https://doi.org/10.1021/acsomega.9b02688
[34] Suhag MH, Khatun A, Tateishi I, et al (2023) One-Step Fabrication of the ZnO/g-C_3N_4 Composite for Visible Light-Responsive Photocatalytic Degradation of Bisphenol E in Aqueous Solution. ACS Omega 8:11824–11836. https://doi.org/10.1021/acsomega.2c06678
[35] Prabhuraj T, Gomathi A, Priyadharsan A, et al (2024) Design of a High-Performance WO3/g-C3N4 Z-Scheme Photocatalyst for Effective Phenol Degradation and Antibacterial Activity. J Clust Sci 35:2753–2768. https://doi.org/10.1007/s10876-024-02692-z
[36] Thangavelu K, Abimannan G, Altaf M, Kumar YA (2025) Designing ZnBi2O4/g-C3N4 Hybrid Nanocomposite Decorated with Enhanced Visible-Light Photocatalytic Activity for Malachite Green Dye Removal. J Clust Sci 36:56. https://doi.org/10.1007/s10876-025-02771-9
[37] Gomathi A, Ramesh Kumar KA, Maadeswaran P (2024) CeO2 nanospheres incorporated with Bi2MoO6/g-C3N4 enhanced photocatalysis towards environmental pollutant Rhodamine B removal. Environmental Science and Pollution Research 31:48103–48121. https://doi.org/10.1007/s11356-024-34073-4
[38] Thangavelu K, Abimannan G, Rajendran R, Arumugam P (2024) Crafting high-performance CuZnO2/g-C3N4 nanocomposites: unleashing the power of dual-functional photocatalysis and antibacterial action. Ionics (Kiel) 30:4885–4899. https://doi.org/10.1007/s11581-024-05603-4
[39] Zhu B, Xia P, Li Y, et al (2017) Fabrication and photocatalytic activity enhanced mechanism of direct Z-scheme g-C 3 N 4 /Ag 2 WO 4 photocatalyst. Appl Surf Sci 391:175–183. https://doi.org/10.1016/j.apsusc.2016.07.104
[40] Farghaly A, Maher E, Gad A, El-Bery H (2024) Synergistic photocatalytic degradation of methylene blue using TiO2 composites with activated carbon and reduced graphene oxide: a kinetic and mechanistic study. Appl Water Sci 14:228. https://doi.org/10.1007/s13201-024-02286-0